BOLETIN DE LA SOCIEDAD ESPAÑOLA DE
Cerámica y Vidrio
www.elsevier.es/bsecv

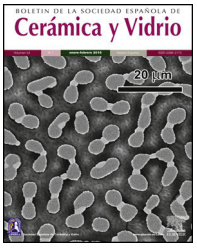

Fabrication and characterisation of ceramics via low-cost DLP 3D printing

Giftymol Varghese[a], *Mónica Moral*[a], *Miguel Castro-García*[a], *Juan José López-López*[b], *Juan Ramón Marín-Rueda*[a,b], *Vicente Yagüe-Alcaraz*[b], *Lorena Hernández-Afonso*[c], *Juan Carlos Ruiz-Morales*[c], *Jesus Canales-Vázquez*[a,*]

[a] *Instituto de Energías Renovables, Paseo de la Investigación 1, Universidad de Castilla-La Mancha, 02071 Albacete, Spain*
[b] *Print3D Solutions, Paseo de la Investigación 1, 02071 Albacete, Spain*
[c] *Dpto. Química, Facultad de Farmacia, Universidad de La Laguna, 38200 Tenerife, Spain*

ARTICLE INFO

Article history:
Received 21 July 2017
Accepted 20 September 2017
Available online 28 October 2017

Keywords:
Ceramics
DLP 3D printing
Photopolymerisation
Photogrammetry
Green body

ABSTRACT

A stereolithography-based additive manufacturing technique has been used for the fabrication of advanced ceramics. A customised 3D printer using a Digital Light Processing (DLP) projector as UV source has been built to fabricate green bodies from photosensitive resins loaded with 25–60 wt% of alumina, 3- and 8-YSZ. The 3D-printed bodies were then sintered in the 1200–1500 °C and exhibited thermal stability. As expected, higher ceramic loadings rendered objects with higher density for a given sintering temperature. The limit of solid loading in the resin is approximately 60% and beyond those contents, the extra ceramic appears as powder loosely adhered to the sintered objects. Photogrammetry was used to evaluate the accuracy of the 3D printing process and highlighted a marked deviation between the CAD model and the resulting object, particularly in the top part of the specimens, possibly due to the use of volatile solvents which cause changes in the photoresins used. Nevertheless, that problem may be overcome by thermostatising the printer vat and/or using solvents with higher boiling point. The results obtained suggest the potential application of low cost DLP 3D printing techniques to process ceramics for a number of applications including ceramic fuel cells, piezoelectrics, dental applications, etc.

Fabricación y caracterización de cerámicas medinate impresión 3D DLP de bajo coste

Palabras clave:
Cerámicos
Impresión 3D DLP
Fotopolimerización
Fotogrametría
Cuerpo verde

RESUMEN

Se ha empleado una técnica de fabricación aditiva basada en la estereolitografía para la producción de cerámicas avanzadas. Se ha diseñado y construido una impresora 3D personalizada empleando como fuente de UV un proyector DLP para fabricar cuerpos verdes a partir de resinas fotosensibles cargadas con el 25-60% en peso de alúmina, 3-YSZ y 8-YSZ. Los cuerpos impresos mostraron estabilidad térmica tras los correspondientes tratamientos de sinterización entre 1.200 y 1.500 °C. Como era de esperar, los mayores contenidos

* *Corresponding author.*
E-mail address: jesus.canales@uclm.es (J. Canales-Vázquez).
https://doi.org/10.1016/j.bsecv.2017.09.004

de sólido en las resinas dieron lugar a objetos con mayores densidades relativas para cada temperatura de sinterización. El límite de carga sólida en las resinas es aproximadamente un 60%, y por encima de estas cantidades, el contenido extra de cerámico aparece como partículas de polvo débilmente adheridas a los objetos sinterizados. Se empleó la fotogrametría para evaluar la precisión del proceso de impresión 3D donde se puso de manifiesto una marcada diferencia entre el modelo CAD y el objeto impreso, especialmente en la parte superior de los especímenes, posiblemente debido al uso de disolventes volátiles que provocan cambios en las fotorresinas empleadas. Sin embargo, este problema puede paliarse termostatizando el contenedor de la resina de la impresora y/o mediante el empleo de disolventes con mayor punto de ebullición. Los resultados obtenidos sugieren la potencial aplicación de técnicas de impresión 3D DLP de bajo coste para el procesado de cerámicos para aplicaciones como pilas de combustible cerámicas, piezoeléctricos, aplicaciones dentales, etc.

Introduction

Ceramics because of their aesthetic value, biocompatibility and physico-chemical properties are highly suitable for biomedical, biochemical and diagnostic applications [1]. Some of the most researched and commonly used bioceramics include pure alumina (Al_2O_3) [2,4,8], pure zirconia (ZrO_2) [3,5,6], alumino-silicates, zirconia doped with yttria, vitreous carbon and calcium phosphate based ceramics [1]. For the past few decades, the chemical composition of the bioceramic was the most relevant parameter, though in recent times the focus has been driven to the relation between processing and the resulting mechanical and thermal properties in order to improve both performance and durability. As a consequence, ceramics such as alumina and zirconia have proved more adequate properties than most metals in implants due to their resistance to corrosion and the ability to withstand very high temperatures [5–7].

In the last 3 decades, additive manufacturing (AM) has emerged as a technology that can be used to fabricate objects with complex geometries straight from a computer-aided design (CAD) file [9,10]. This group of techniques may be applied to a wide range of materials, from polymers to metals and also ceramics [1]. Although it was first conceived for rapid prototyping, 3D printing has undergone outstanding progress and becomes gradually more popular, particularly due to some advantages compared to other manufacturing techniques as is the possibility of fabricating complex geometries, rational use of materials, relatively low time consumption and they can be user friendly. AM includes a number of technologies such as Selective Laser Sintering (SLS), Fused Deposition Modelling (FDM), Stereolithography Apparatus (SLA), Inkjet-Based Systems and others [9]. In the case of ceramics, FDM may not provide enough resolution for applications where a good finish is required such as odonthology or electroceramics as the nozzle tends to be rather large. Inkjet technologies have already been used in ceramics with very good results, although it may be time-consuming when printing out objects others than thin films or high aspect ratio structures. SLS has been reported as an adequate technique for high quality ceramics, although the systems are rather expensive. In the case of SLA, there are rather economic systems to produce ceramics with high output resolution and surface quality [9–12], and moreover the systems could be customised by replacing the laser and using DLP projectors which can also produce high quality ceramics at low cost [13].

Regarding SLA 3D printing of ceramics, Al_2O_3-based resins were characterised by Brady et al. to rapid prototype ceramics with the assistance of a SLA machine [11] and later some ceramic systems were studied [17]. Since then, there has been some progress in this field as reviewed by Ferrage et al. [14]. In that work, the effect of processing upon the control of porosity and prevent the appearance of cracks was pointed out. In any case, most of those works refer to high profile 3D printers and they appear to be restricted to just a few materials. As yttria-stabilised zirconia has its relevance in a range of commercial and industrial sectors and can be efficiently manufactured and characterised, that offered us the motivation to present this novel work on low cost SLA-based manufacturing of alumina, 3 and 8 mol% YSZ. As 3D printed ceramic objects are obtained after the modelling of the geometrical bodies in a CAD software, it is highly relevant to correlate the dimensions of the printed object compared to the original model. In the present study, we have attempted to apply classic photogrammetry and Structure-form-Motion (SfM) algorithm to estimate accurately the changes in the dimensions of the ceramics during the 3D printing process by 3D reconstruction. This classic photogrammetric process is carried out by image acquisition, image measurement using a series of target points with known 3D positions and processing which involves aligning the target points for object reconstruction [15]. On the other hand, in SfM, the geometry of the object, camera positions and orientation are solved automatically without the need to specify a network of targets [16].

Materials and methods

Material preparation and processing

Ceramic-loaded photosensitive resins were prepared using 25–60% (w/w) of alumina (Sigma–Aldrich), 3 and 8% YSZ (Kingda Ceramics), poly(ethylene glycol) diacrylate (Sigma–Aldrich), a UV photo initiator (PI) phenyl bis (2,4,6-trimethyl(benzoyl)phosphine) in 5 ml of an organic solvent

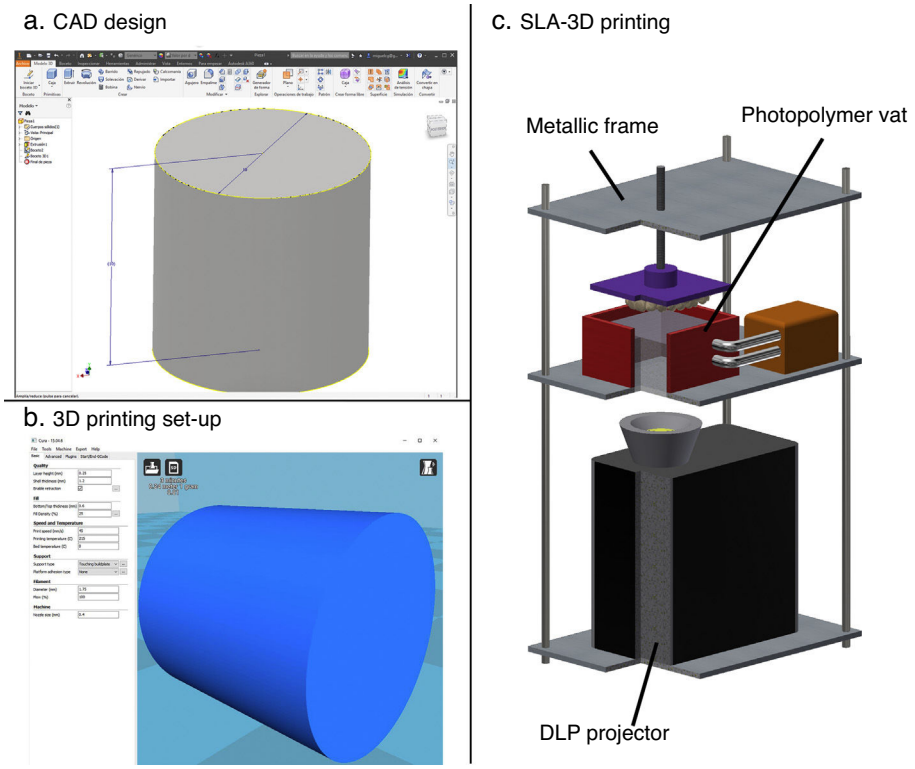

Fig. 1 – Schematic representation of the process which includes modelling, slicing and 3D printing.

(typically ethanol) for every 10 g of the sample. The ingredients were kept under mild stirring for 2 h until a slurry was obtained, which was subsequently ballmilled for 6 h in a Pulverisette7 FRITSCH planetary ballmill at 200–400 rpm. As ballmilling for long periods of time could result in solvent evaporation, the zirconia containers were sealed throughout the process to keep the solvent to solid ratio constant.

DLP 3D printing

In this work a modification of conventional SLA 3D printers was developed by Print3D Solutions to print out the ceramic slurries previously described. The UV source used to carry out the research presented in this work was a HDMI 3D-FULL HD 1080 DLP projector manufactured by Texas Instruments, emitting UV light at 380 nm. The printing apparatus comprised of a metallic platform and a photopolymer pool/vat of a building envelope 82.35 mm × 47.10 mm × 144 mm, with a Teflon base capable to hold the photoactive resin loaded with ceramic powders. The model designed in Computer Aided Engineering (CAE) software (Autodesk Inventor Professional, USA) (Fig. 1a), planned in the *stl* file (Fig. 1b) is then virtually sliced into layers of a pre-defined thickness. The subsequent information is translated into G-code, which is a numerical control programming language for automated machines (Fig. 1c), to re-create layer-by-layer, the original model. With the assistance of a 3D printer control software, i.e. Creation Workshop, the DLP projector draws an outline on to the surface of the photopolymer vat, fixed to the holders on the *X* and *Y*-axis of the printer. The metallic platform tightly screwed to a movable stage on the *Z*-axis of the printer acts as a lift device, maintaining a lift distance of 4 mm from the pool. Due to the exposure to UV light, the resin is cured (photopolymerisation process) and consequently hardens and adheres the first layer to the platform [16]. In the subsequent immersion of the platform in to the pool, uncured liquid ceramic-loaded resin from the vat clears over the first layer, coating it with fresh material. That second layer is polymerised again by UV light and adheres to the previous layer. The process is repeated until the complete model is reproduced. In the present work, the layer thickness was 25–50 μm. When the 3D object has been completed, it is scraped off the platform, giving an output resolution of approximately 45 μm *X*- and *Y*-axes. When working with vat 3D printing technologies, both SLA and DLP, there are two possible ways to fabricate the object: from top to bottom or from bottom to top. Top to bottom is usually preferred in SLA systems as problems associated with light dispersion are minimised. In the present case, bottom to top has been chosen as one may 3D print even if the vat is not full of resin, potentially decreasing the cost of the experiments, whereas in top to bottom configurations the vat must be completely filled. Additionally, the use of a Teflon layer allows the pass of the UV radiation from the projector with negligible dispersion.

Simple test structures such as cubes and closed cylinders of different dimensions were modelled and 3D printed. During their fabrication, the UV exposure time set for the bottom 4 layers was 70–80 s to ensure good adhesion to the platform and 5–7 s for the next layers. The layer thickness, curing time and the grid adjustments had to be carefully monitored to avoid any discontinuity in the process or dispachtment of layers from the platform. Once the structures were built, they underwent a chemical washing (typically butanol or propanol)

to remove the excess material, followed by a curing time of about 2–4 min under a UV lamp emitting a light of wavelength 253 nm. The so-obtained green bodies were then dried in a stove at 60 °C for 6–12 h and then at 140 °C for 3 h to remove all the volatiles. After that, the ceramics were sintered from 1200 to 1500 °C for 6 h at 5 °C/min. In the case of alumina and 3-YSZ this procedure was adequate to produce good quality ceramics. In the case of 8-YSZ, this procedure led to the formation of cracks upon sintering and therefore an alternative debinding route was considered. In the case of 8-YSZ, after drying at 60 °C, samples were fired under reducing conditions (5%H_2/Ar) at 450 °C for 6 h at 2 °C/min.

Materials characterisation

XRD was used to evaluate the phase changes that may occur upon 3D printing, postprocessing and further sintering. The experiments were performed in a PANalytical diffractometer equipped with a X'Celerator detector with monochromatic CuKα1 radiation (λ = 1.54056 Å). XRD patterns were performed in the 10–70° 2θ range.

Thermogravimmetric analysis (TGA) of the green bodies was analysed using a Jupiter STA 449C (Netzsch) thermobalance in flowing air (25 ml/min). A blank was run to calibrate the background and after that a small portion (around 40 mg) of the green body was placed in one of the crucibles and heated up from 50 °C to 600 °C at a ramp rate of 5 °C/min.

The microstructure of the sintered bodies was studied via SEM. The SEM microscope used in this work was a JEOL JSM-6490LV (Tokyo, Japan) equipped with EDS (Oxford Link) and detector for backscattered electrons, operating between 0.1 kV and 30 kV. The ceramics examined under the SEM were sputter coated with non-oxidising metals such as Au-Pt using a SC7620 sputter coater by EMITECH to improve their conductivity and avoid charging-up problems and therefore improve image definition.

Geometrical analysis

To evaluate the accuracy of the 3D printing process, several cylinders (*d*: 10 mm, *h*: 10 mm) were fabricated from resins containing 45–55% 3-YSZ. A combination of the classic photogrammetric and SfM was operated on a custom-made photogrammetric set-up, to acquire multiple images of the point of interest on the object from different camera positions and further process them by overlapping the images and aligning the reference points to reconstruct the 3D image. This 3D scan does not work like black boxes as occurs for commercial 3D scanners as they do not provide tools to evaluate the quality of the object [15]. Pictures of the sintered bodies were taken using a Nikon D3200 digital camera held on a tripod stand at a minimal distance from the object of interest. Target points were drawn on the platform with the object placed on it to scale the model and control the quality of the 3D reconstruction. 72 pictures of the object were captured. The images must overlap at least 80% in order to measure the parallaxes [16], which is the displacement in the position of an object viewed from two different points of observation. Further, 3D points deduced from the 2D image from different camera positions were fed into the photogrammetric processor that is capable of generating a 3D model from them, enabling the user to navigate through them easily. The so-reconstructured images in

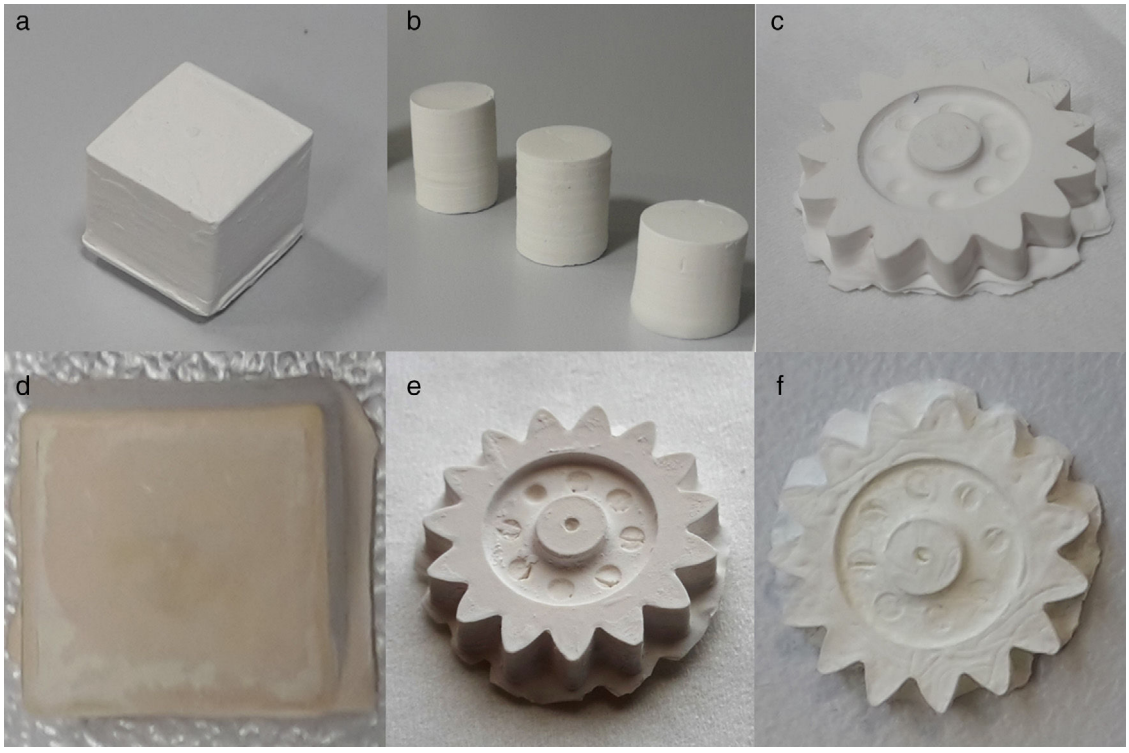

Fig. 2 – Green bodies of photo resin loaded with 55% 3-YSZ (a, b, c). Brown bodies after drying at 140 °C (d, e). After sintering at 1500 °C (f).

the 3D model gave us accurate information of the area and the volume of the sintered objects which were compared with that of their original 3D designs in order to measure the accuracy of the 3D printing process.

The original cloud of points (ORIG) is treated to obtain the capture base plane (which coincides with the base of the 3D printed object attached to the printing platform) and the cylinder matching the 3D mesh of the printed object (FITTED). To achieve this, the qRansacSD stands algorithm developed by Schnabel et al. [18] was used. Models are calculated from the centre of the FITTED cylinder and considering as base the horizontal plane of the reference cylinder (REF) with the same origin point.

Results and discussion

During resin preparation, homogenisation of the raw material became a highly relevant stage to improve the sintering properties of the final objects. Increasing the ballmill speed and milling time led to stable homogeneous suspensions adequate to get attached to the printing platform. If the suspensions exhibited well-defined separated phases, the 3D printing process could not be carried out and deleterious effects such as delamination occurred. Taking this into account, we were able to produce well-defined layered structures with tailored finish and minimum crack propagation (Fig. 2). The printing apparatus had to be adjusted tight to the fixtures to avoid a slanted built frame, also called the staircase effect [19,20].

The TGA analysis of the green body revealed information on the decomposition behaviour of the organic matter with the changing temperature. From the graphical representation given in Fig. 3, it is evident that in the 140–200 °C temperature range, all the volatile solvent gets evaporated from the green body as suggested by the gentle decay of the TG curve. From that temperature, decomposition of the resin occurs in 2 steps with an exothermic reaction that peaks at 375 °C, and then the remaining organic matter (5–7%) is eliminated in a strongly exothermic process which peaks at 480 °C, leaving only the ceramic inside the printed part. The TGA experiments were run for a range of ceramic loadings and they all exhibited almost identical behaviours. It should be noted in Fig. 2, that the mass percent achieved post the decomposition of all the organic matter from the green body was almost the same as

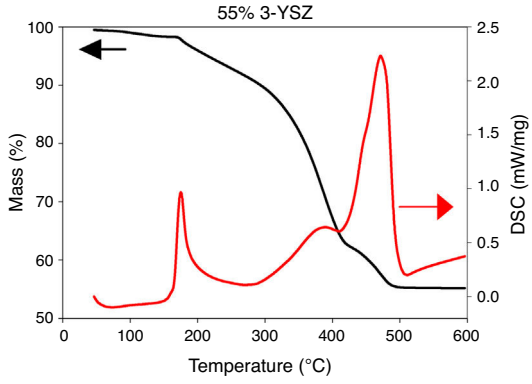

Fig. 3 – TGA/DSC curves corresponding to the photoresin loaded with 55% of 3-YSZ.

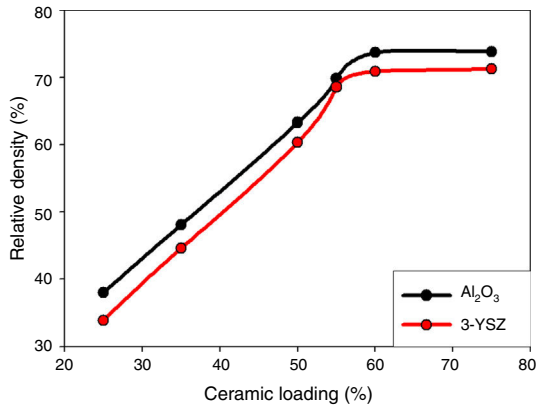

Fig. 4 – Evolution of the relative density vs ceramic loading in 3D printed cubes sintered at 1500 °C for 6 h (ramp rate 5 K min^{-1}).

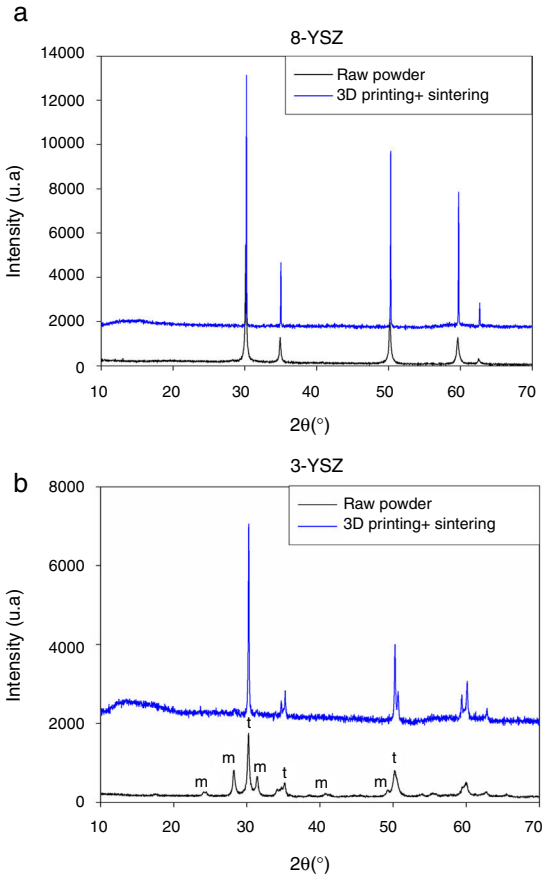

Fig. 5 – XRD patterns of 8-YSZ (a) and 3-YSZ (b) as raw powder and after 3D printing process and sintering at 1500 °C. m denotes monoclinic and t tetragonal in the case of 3-YSZ.

that of the original mass percent of the ceramic in the photoactive resin. This indicates that there are no significant solvent losses during post processing. In our initial experiments, after the 3D printing process, the green bodies were fired directly at high temperatures, which resulted in complete crashing of the objects. After analysing the TGA on the green bodies, the

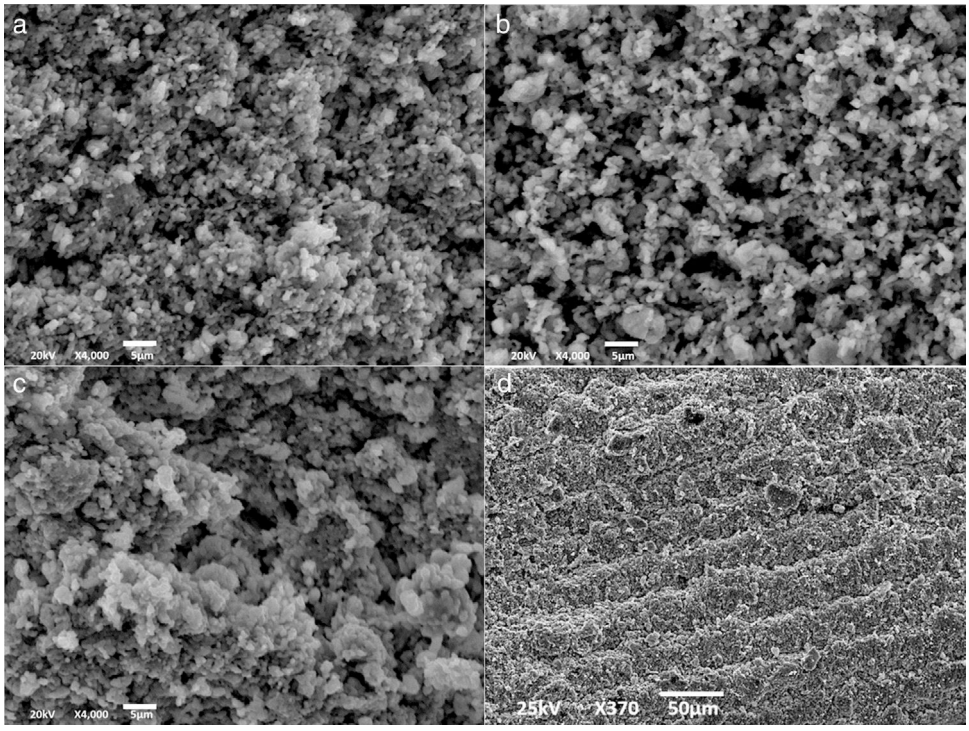

Fig. 6 – SEM micrographs of 3D printed 3-YSZ sintered at 1200 °C: (a) 25%, (b), 45%, (c) 60% 3YSZ loading, (d) cross-sectional view of 60% 3-YSZ.

sintering process included a previous drying stage to evaporate the volatile solvents at 140 °C. At that temperature solvents are removed, and resin starts to decompose leading to a brown body, which can be sintered at high temperatures rendering objects without delamination or cracks.

The printing process occurs when the diacrylate monomers and oligomers polymerise when exposed to the UV radiation in the presence of the PI. As the target in this case is to print out a polymer-ceramic composite, it is very important to determine the range of ceramic loadings that lead to printable resins. Under our experimental conditions, loadings below 25% weight of ceramic resulted in printable resins, though upon sintering the structures collapsed. Higher ceramic loadings allow the fabrication of objects which retain their morphology upon sintering. When analysing the resulting relative density of the 3D printed ceramics as a function of the ceramic loading for a given sintering temperature, higher solid loadings render gradually higher final relative densities up to 55–60%. At that point, higher ceramic contents do not render denser objects and therefore it could be considered as the saturation point (Fig. 4). It should be noted that adding higher ceramic loadings result in sintered objects covered with loose powder, which may be interpreted as further evidence of the saturation point of the photoresins used in the present work. Higher densities may be achieved via modification of the sintering treatments, e.g. using higher sintering temperatures for prolonged periods of time, modification of the photoactive resin to include organic binders or even debinding under non-oxidising conditions [21].

XRD experiments were performed on both the raw powders and the objects after sintering to monitor whether any phase changes occur upon the entire process. In the case of alumina and 8-YSZ no changes were observed and the original phases were retained throughout the process (Fig. 5a). On the other hand, 3-YSZ was originally a 50:50 mixture of monoclinic and tetragonal zirconia and after sintering the powders had evolved to tetragonal zirconia mostly although some cubic peaks can also be detected (Fig. 5b). A similar behaviour has been observed when sintering the raw 3-YSZ powders. These results indicate that the 3D printing process does not have any impact in phase stability compared to more conventional processing techniques.

We analysed the SEM images of the 3D printed specimens with ceramic loadings varying from 25 to 60%, sintered for 6 h in the 1200–1500 °C temperature range, using a ramp rate of 5 °C/min. The results were similar for alumina, 3-and 8-YSZ. The SEM micrographs in Figs. 6–9 all correspond to 3-YSZ for comparison. It is clear that the lowest sintering temperature, i.e. 1200 °C, renders poorly sintered microstructures with high porosity and small grain size (Fig. 6). The highest ceramic loadings render somewhat denser microstructures although it is rather difficult to discern just by SEM. The layers at the crossection, although defined, are covered with unsintered 3-YSZ grains. A similar situation was found at 1300 °C with somewhat better defined grains (Fig. 7). As the sintering temperature increases, i.e. 1400 °C (Fig. 8) the grain appears clearly defined and their size is notably larger and the microstructure is more compact. The cross-sectional view (8d) appears much better resolved as a result. In the case of specimens sintered

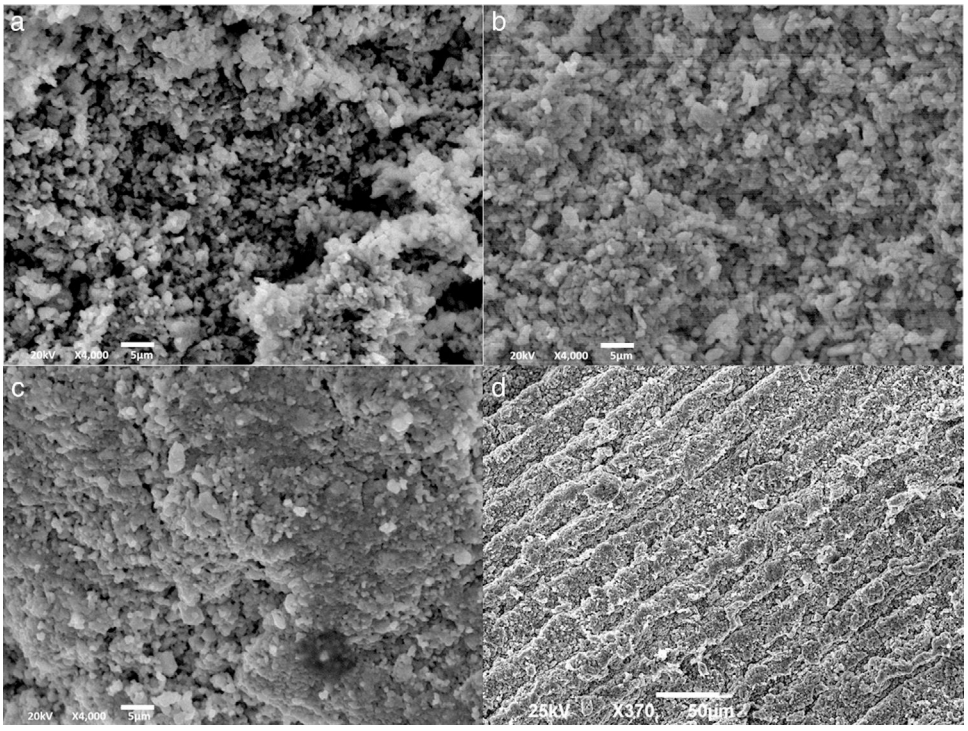

Fig. 7 – SEM micrographs of 3D printed 3-YSZ sintered at 1300 °C: (a) 25%, (b) 45%, (c) 60% 3YSZ loading, (d) cross-sectional view of 60% 3-YSZ.

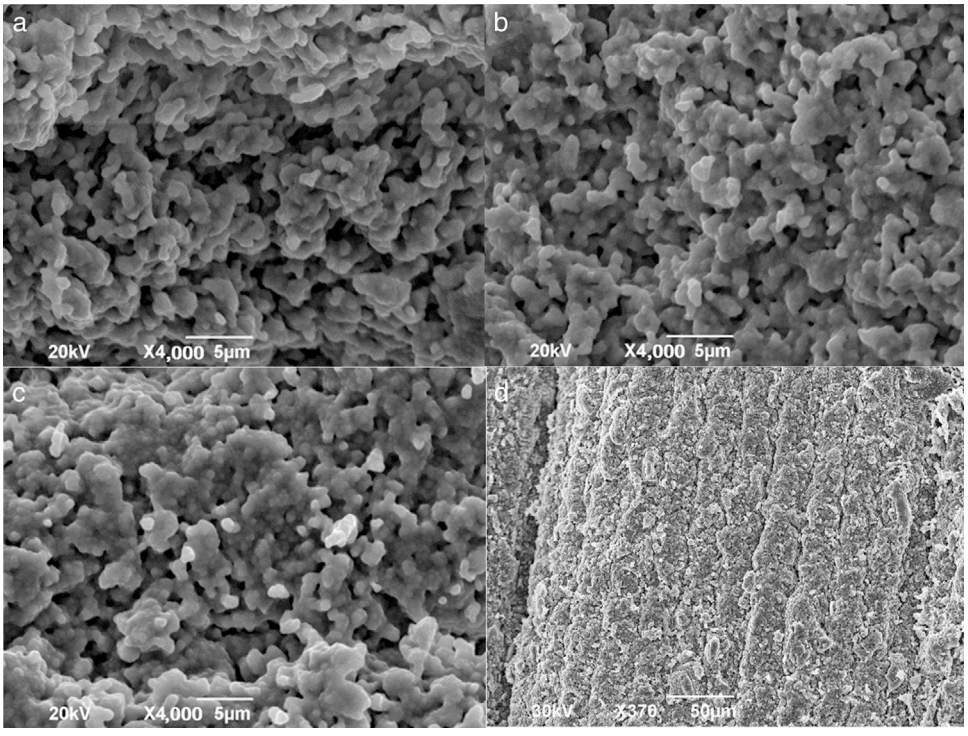

Fig. 8 – SEM micrographs of 3D printed 3-YSZ sintered at 1400 °C: (a) 25%, (b) 45%, (c) 60% 3YSZ loading, (d) cross-sectional view of 60% 3-YSZ.

at 1500 °C a distinguishable dense packing of the grains were observed (Fig. 9), displaying a much more compact microstructure compared to those sintered at lower temperatures. As mentioned above, higher solid loadings did not render higher densities as the extra ceramic appear loosely adhered to the surface rather than being a part of the specimen.

Another remarkable effect of sintering on the microstructure of ceramics is the shrinkage which also affects to the

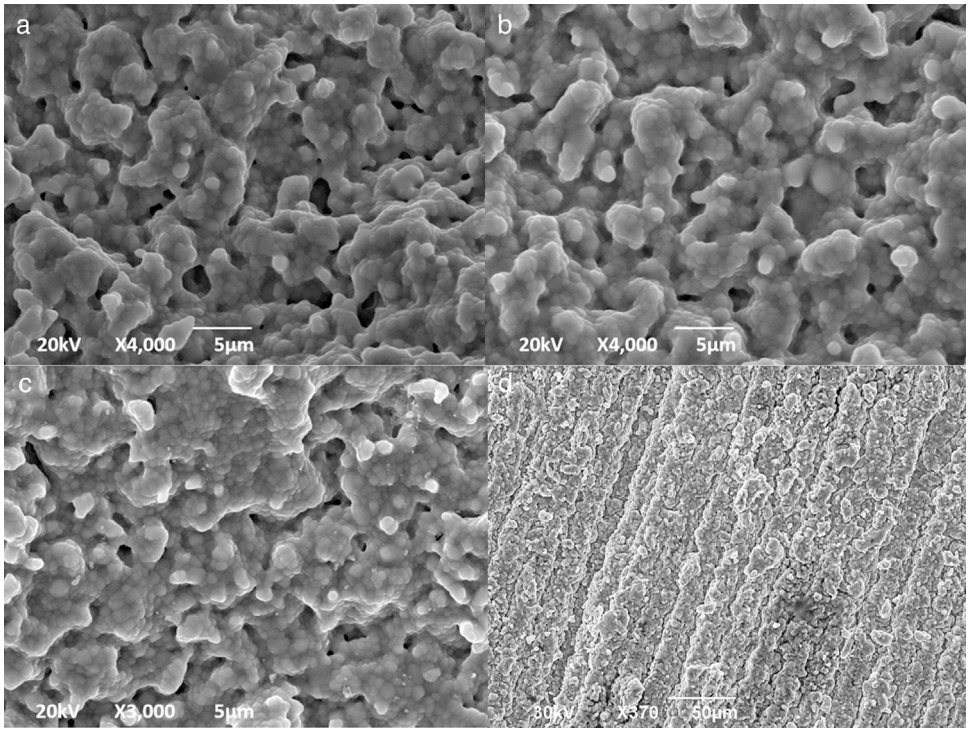

Fig. 9 – SEM micrographs of 3D printed 3-YSZ sintered at 1400 °C: (a) 25%, (b) 45%, (c) 60% 3YSZ loading, (d) cross-sectional view of 60% 3-YSZ.

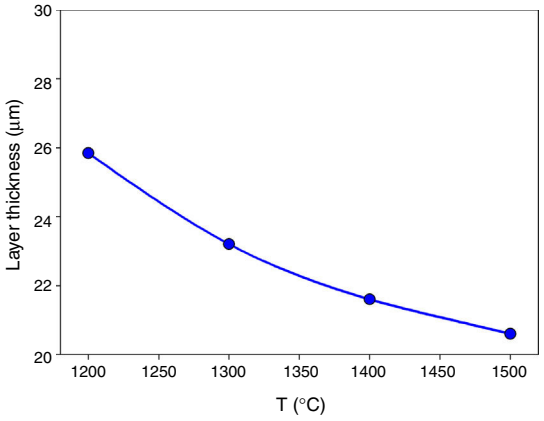

Fig. 10 – Evolution of the layer thickness as a function of the sintering temperature. Layer thickness in the 3D printed green bodies was set at 50 µm in all cases.

layer thickness and therefore to the resolution along the z-axis. In the case of polymers, the resolution along the z-axis depends on the layer thickness, which is a parameter that can be defined by the user. In the case of ceramics, the final layer thickness will also depend on the sintering process, which in turn depends on the ceramic loading, temperature, time, ramp rate, etc., as discussed above. To illustrate this, several cylinders containing 60% of 3-YSZ were 3D printed with a layer thickness of 50 µm and then fired at 1200 °C, 1300 °C, 1400 °C and 1500 °C for 6 h at a 5 K min^{-1} ramp rate. The contraction of the layers was large in all cases and became gradually larger upon increasing the temperature as shown in Fig. 10. In other words, the resolution along the z-axis may be reduced upon sintering in the case of ceramics. Analogously contraction along the *xy* plane also occurs, typically 50–60% when firing up 3- and 8-YSZ at 1400 and 1500 °C for 6 h, which is higher than in the case of pressed raw powders. Nevertheless further research must be performed to discern whether such dimensional changes may affect the properties of the resulting ceramics.

As mentioned in the experimental section, photogrammetry and SfM were used to evaluate the accuracy of the 3D printing process. As shown in Table 1 and Fig. 11, there exists a marked deviation from the CAD model and the resulting 3D printed cylinders. Nevertheless the analysis of the distances between the equivalent cylinder (FITTED) and the reconstructed 3D model (ORIG) is homogeneous along the bodies. Several aspects must be highlighted: first, the central parts of the cylinders show rather small deviations, whereas the bases exhibit much larger deviations and the aspect is far more irregular. Indeed, parallelism is lost in the top part of the cylinders compared to the bottom base. One may think that such deviation between the printed object and the model is due to poor quality of the printing. However, previous work on commercial polymeric resins using the same DLP printer did not show such deviations. Therefore, the discrepancy between model and green body must be related to processing parameters. The ceramic-loaded resins used in the present work contain rather volatile solvents (ethanol). Ethanol evaporates upon the printing process as the UV source heats gradually the vat containing the resin (at an estimated rate of 4 °C/h) and moreover the postprocessing implies washing with alcohols

Table 1 – Area, volume and shrinkage values from REF and FITTED cylinders.

	Reference CAD model		Fitted green body model		Green body shrinkage		
	Area (mm^2)	Volume (mm^3)	Area (mm^2)	Volume (mm^3)	Area (%)	Volume (%)	V/A
C2-45%	471.24	785.40	348	490.99	26.2	37.5	1.43
C2-55%	471.24	785.40	430.65	685.63	8.6	12.7	1.48
C3-45%	471.24	785.40	410.96	639.39	12.8	18.6	1.45
C3-45%	471.24	785.40	396.91	602.35	15.8	23.3	1.47

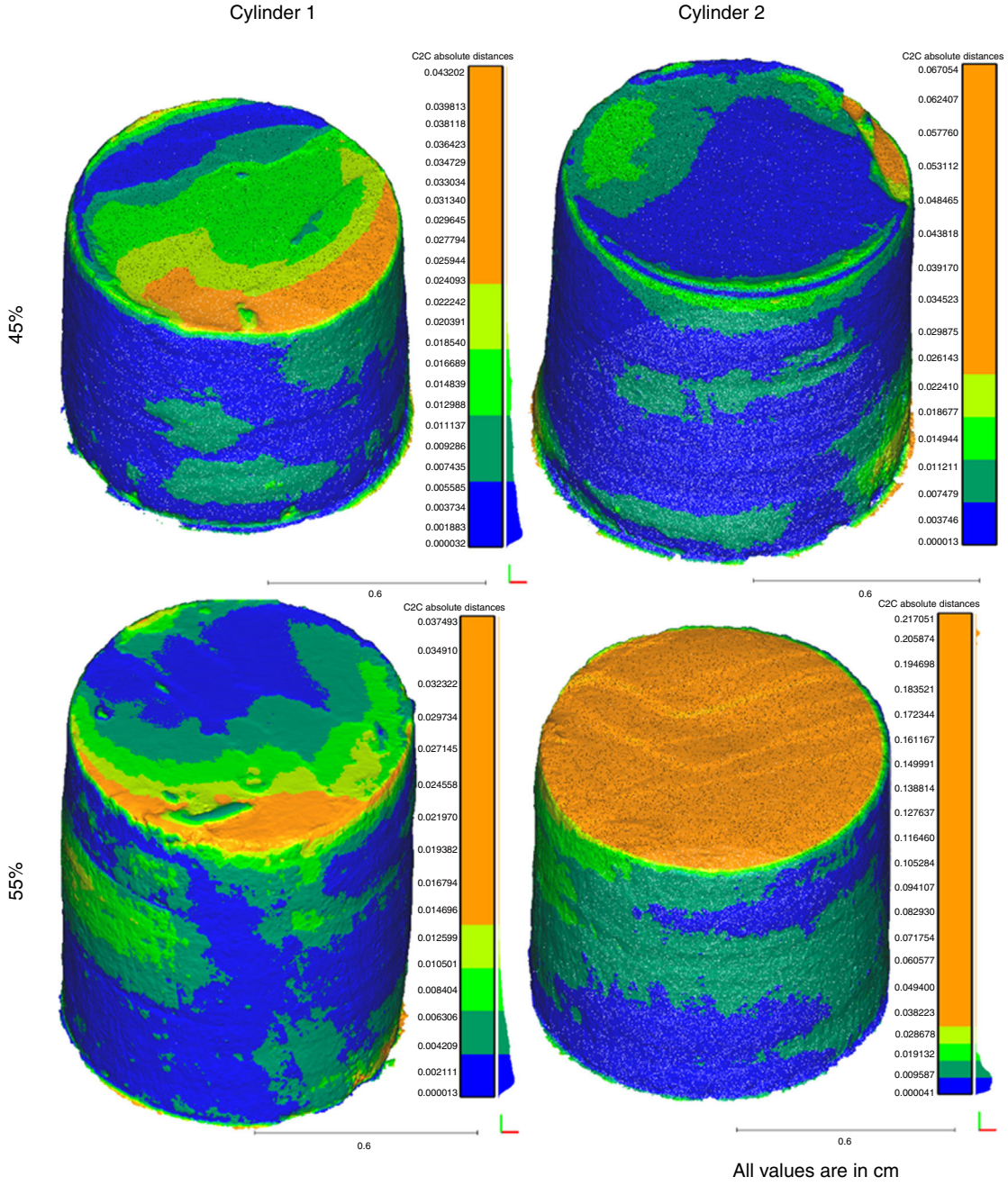

Fig. 11 – Distance analysis of the cloud points ORIG vs. FITTED for 4 green bodies cylinders.

and UV exposure (local heating). In other words, the printing conditions are modified during fabrication and to make things worse the green body loses volatiles. The sintering process does not mitigate that effect and indeed, some of the samples sintered at high temperatures exhibit irregular surfaces especially on the top base (Fig. 2f). To minimise these effects, several strategies may be applied. For instance, ethanol could be replaced by alcohols exhibiting a higher

boiling point as is the case of 2-butanol. Another interesting approach would be a modification in the DLP printer vat to couple a refrigeration system to keep the temperature constant throughout the entire 3D printing process.

Conclusions

In this work we present a low-cost DLP-based 3D printing technique as a potential manufacturing technique for highly relevant ceramics such as alumina, 3-YSZ and 8-YSZ. Photoactive resins for the 3D printing process were prepared by mixing 25–60 wt% ceramic with poly (ethylene glycol) diacrylate and a photoinitiator dissolved in ethanol that after exposure to the UV light from a commercial DLP projector rendered cured layers of a polymer-ceramic composite. The 3D object is generated by piling up consecutive layers that after drying and sintering render specimens with thermal stability. The ceramic loading in the resin plays a relevant role, which a direct effect on the final density of the ceramic. Nevertheless, there is a saturation point at approximately 60% ceramic loading, where the extra ceramic powder does not get in to the photoresin and hence appears as a loose powder badly adhered to the surface of the sintered object. Further improvement in the sintering process may be achieved by modifying the debinding conditions, which will be the subject of a future work.

Photogrammetry and SfM were used to evaluate the accuracy of the 3D printing process and revealed discrepancies between the CAD model and the green body obtained, especially in the top part of the specimens, i.e. corresponding to the last layers. As the solvent used in the present work was very volatile and the temperature increased gently during the experiments, the properties of the photoresin are changing as well and that could perfectly explain the deviations observed. Nevertheless, this methodology has proven a relatively simple and elegant way to determine the real geometry of the printed objects and further comparison with the original models.

Acknowledgements

The authors acknowledge technical support provided by the UCLM spin-off company Print3D Solutions SL and E2TP-CYTEMA Santander for funding.

REFERENCES

[1] N. Huebshch, D.J. Mooney, Inspiration and application in the evolution of biomaterials, Nature 462 (2010) 426–432.
[2] J.J. Yoon, M.P. Chun, S. Nahm, Fabrication and characterization of alumina-TZP (3Y) composite ceramics, J. Korean Inst. Electr. Electron. Mater. Eng. 28 (3) (2015) 170–174.
[3] C. Piconi, G. Maccauro, Zirconia as a ceramic biomaterial, Biomaterials 20 (1) (1999) 1–25.
[4] J.E. Lemons, Dental implants biomaterials, J. Am. Dent. Assoc. 121 (6) (1990) 715–718.
[5] T. Vagkopoulou, S.O. Koutayas, P. Koidis, J.R. Strub, Zirconia in dentistry: part 1. Discovering the nature of an upcoming bio ceramic, Eur. J. Esthet. Dent. 4 (2) (2009) 135–161.
[6] N. Demir, M.G. Subaçi, A.N. Ozturk, Surface roughness and morphologic changes of zirconia following different surface treatments, Photomed. Laser Surg. 30 (6) (2012) 341–345.
[7] J. Chevalier, What future for zirconia as a biomaterial? Biomaterials 27 (4) (2006) 540–543.
[8] T. Shirai, H. Watanabe, M. Fuji, M. Takahashi, Structural Properties and Surface Characteristics on Aluminum Oxide Powders, Ceramics Research Laboratory, Nagoya Institute of Technology, 2009, pp. 23–31.
[9] D. Banoriya, R. Purohit, R.K. Dwivedi, Modern trends in rapid prototyping for biomedical applications, in: 4th International Conference on Materials Processing and Characterization, 2015, pp. 3409–3411.
[10] J.C. Ruiz-Morales, A. Tarancón, J. Canales-Vázquez, J. Méndez-Ramos, L. Hernández-Afonso, P. Acosta-Mora, J.R. Marín Rueda, R. Fernández-González, Three dimensional printing of components and functional devices for energy and environmental applications, Energy Environ. Sci. 10 (2017) 846–859.
[11] G.A. Brady, J.W. Halloran, Stereolithography of ceramic suspensions, Rapid Prototyp. J. 3 (2) (1997) 61–65.
[12] L. Ruiz, M.J. Readey, Effect of heat treatment on grain size, phase assemblage, and mechanical properties of 3-molpercentage Y-TZP, J. Am. Ceram. Soc. 79 (1996) 2331–2340.
[13] E.M. Hernández-Rodríguez, P. Acosta-Mora, J. Méndez-Ramos, E. Borges Chinea, P. Esparza Ferrera, J. Canales-Vázquez, P. Núñez, J.C. Ruiz-Morales, Prospective use of the 3D printing technology for the microstructural engineering of solid oxide fuel cell components, Bol. Soc. Esp. Ceram. Vidr. 53 (5) (2014) 213–216.
[14] L. Ferrage, G. Bertrand, P. Lenormand, D. Grossin, B. Ben-Nissan, A review of the additive manufacturing (3DP) of bio ceramics: alumina, zirconia (PSZ) and hydroxyapatite, J. Aust. Ceram. Soc. 1 (2016) 42–56.
[15] F. Remondino, M.G. Spera, E. Nocerino, F. Menna, F. Nex, State of the art in high density image matching, Photogramm. Rec. 29 (2014) 144–166.
[16] G.J. Grenzdörffer, M. Guretzki, I. Friedlander, Photogrammetric image acquisition and image analysis of oblique images – a new challenge for the digital airborne system PFIFF, Photogramm. Rec. 12 (2008) 372–386.
[17] F. Doreau, C. Chaput, T. Chartier, Stereo lithography for manufacturing ceramic parts, Adv. Eng. Mater. 2 (2000) 493–496.
[18] R. Schnabel, R. Wahl, R. Klein, Efficient RANSAC for point-cloud shape detection, Comput. Graph. Forum 26 (2) (2007) 214–226.
[19] N. Travitzky, A. Bonet, B. Dermeik, T. Fey, I. Filbert-Demut, L. Schlier, T. Schlordt, P. Greil, Additive manufacturing of ceramic-based materials, Adv. Eng. Mater. 16 (6) (2014) 729–754.
[20] N. Guo, M.C. Leu, Additive manufacturing: technology, applications and research needs, Front Mech. Eng. 8 (3) (2013) 215–243.
[21] P. Thomas-Vielma, A. Cervera, B. Levenfeld, A. Várez, Production of alumina parts by powder injection molding with a binder system based on high density polyethylene, J. Eur. Ceram. Soc. 28 (4) (2008) 763–771.